Photoinjection of fluorescent nanoparticles into intact plant cells using femtosecond laser amplifier

Taufiq Indra Rukmana, Gabriela Moran, Rachel Méallet-Renault, Gilles Clavier, Tadashi Kunieda, Misato Ohtani, Taku Demura, Ryohei Yasukuni, Yoichiroh Hosokawa

Photoinjection of fluorescent nanoparticles into intact plant cells using femtosecond laser amplifier

Taufiq Indra Rukmana,1 Gabriela Moran,2 Rachel Méallet-Renault,2 Gilles Clavier,3 Tadashi Kunieda,4 Misato Ohtani,4,5 Taku Demura,4 Ryohei Yasukuni,1,a) and Yoichiroh Hosokawa1

AFFILIATIONS

1 Division of Materials Science, Graduate School of Science and Technology, Nara Institute of Science and Technology,

630-0192 Ikoma, Japan

2Université Paris-Saclay, CNRS, Institut des Sciences Moléculaires d'Orsay, 91405 Orsay, France

3Université Paris-Saclay, ENS Paris-Saclay, CNRS, PPSM, 94235 Cachan, France

4Division of Biological Science, Graduate School of Science and Technology, Nara Institute of Science and Technology,

630-0192 Ikoma, Japan

5Department of Integrated Biosciences, Graduate School of Frontier Sciences, The University of Tokyo, 277-8562 Chiba, Japan

a)Author to whom correspondence should be addressed: r-yasukuni@ms.naist.jp

ABSTRACT

The introduction of nanoparticles to intact plant cells is promising as a transporting technique of a wide range of functional molecules. Among various molecular delivery methods, femtosecond laser photoinjection possesses target selectivity at a single cell level and is potentially applicable for many types of materials. However, for plant cells, the vacuoles' turgor pressure and the thick cell wall limit the application of photoinjection to only small objects. In this work, we overcome these limitations by employing a single pulse irradiation from a femtosecond laser amplifier. After laser irradiation on intact tobacco BY-2 cells, 80 nm fluorescent nanoparticles dispersed in a cell culture medium were successfully injected into their cytoplasm. This breakthrough would lead to a vast utilization of nanoparticles containing functional molecules for single cell manipulation in plant physiological study and genetic engineering. Such an injection was observed even when the laser pulse was focused neither on the cell wall nor on the cell membrane, but beside the cells. With these results, we suggest pore formation on the cell membrane by instantaneous deformation induced by an intense femtosecond laser pulse as an injection mechanism of nanoparticles. Reported photomechanical effects of the amplified femtosecond laser on the permeability of the biological membrane would offer new perspectives in biophotonics.

I. INTRODUCTION

The introduction of nanoparticles to intact plant cells is a promising technique in agriculture and plant physiological study. Thanks to unique characteristics of nanoparticles such as accumulation behavior in a specific area and release control of encapsulated molecules, they take a role as transporters for a wide range of functional substances from small agrochemicals (fertilizers, pesticides, herbicides, etc.) to large proteins and DNA.1–3

The introduction of nanoparticles into intact plant cells is generally managed either by diffusion through the plant cell wall or by active uptake mediated by cellular processes.4–6 The introduced nanoparticles are then transported to other plant organs. However, the applicability of such passive methods is highly material dependent. As a physical approach, particle bombardment also allows delivery, through cell walls, of gold or tungsten nanoparticles coated with genetic molecules (DNA, RNA, etc.).6,7 The main drawbacks are low introduction efficiency and damage of target samples or delivered molecules.8–11 Herein, our attention is directed to a laser-assisted injection technique called photoinjection. In this method, molecules are injected through a pore formed by laser irradiation on a cell. Photoinjection possesses target selectivity at a single cell level with high throughput and it is applied to various materials.12–16 These features are significantly important to reveal spatiotemporally complex plant systems such as cell–cell communications.17

In animal cells, photoinjection of various kinds of functional molecules including large DNA plasmids and their expression is achieved by employing the femtosecond (fs) laser, which permits high-efficiency and high-precision cells and tissues-processing.18–22 On the other hand, the application of photoinjection to plant cells is restricted. Indeed, unlike animal cells, turgor pressure originated from the osmotic flow of water to plant vacuoles keeps inner pressure at a higher level that prevents injection through the molecular diffusion process. Another limitation is the presence of thick and rigid cell walls. The cell wall blocks large molecules typically larger than 5 nm.23,24 In the previous reports, although small molecules were successfully injected into intact plant cells by fs laser irradiation under osmotic pressure control, injection of larger molecules than about 5 nm had not yet been attained.23,24

We have recently applied single pulse irradiation from fs laser amplifier with higher energy than the previous photoinjection reports.25 With this fs laser irradiation scheme, large 2 MDa molecules were injected into a target tobacco BY-2 (TBY-2) cell. In addition, the photoinjection efficiency was enhanced by adjunctive enzyme treatment, which increased permeability of the cell wall. Although their injection mechanism by the intense fs laser pulse was not fully understood, they showed the potential of injecting larger substances into single plant cells with cell walls.

In this work, we examined the applicability of the photoinjection using the fs laser amplifier to nanoparticles into a single TBY-2 cell. The photoinjection efficiency of the nanoparticles was investigated from the aspect of cellular conditions and laser irradiation parameters. Moreover, the photoinjection mechanism of nanoparticles was discussed based on a photomechanical effect, which is effectively induced by using the fs laser amplifier.

II. METHODS

A. Preparation of tobacco BY-2 cells

Wild-type TBY-2 cells were prepared using the slightly modified method from previous reports.25–27 The TBY-2 cell culture medium contains 4.6% (w/v) of Murashige–Skoog (MS) basal medium (Ducheva Biochemie) containing 3% (w/v) of sucrose (Sigma-Aldrich), 0.2 g/l of KH2PO4 (Sigma-Aldrich), 1 mg/l of thiamine-HCl (Sigma-Aldrich), 100 mg/l of myo-inositol (Sigma-Aldrich), and 0.1 mg/l of 2,4-dichlorophenoxyacetic acid (Sigma-Aldrich). The cultured cells were incubated on a rotary shaker (130 rpm) in a dark room at 27 °C. Every 7 days, 2 ml of the cell suspension was transferred into 95 ml of new medium for sub-culturing.

Two-day old cultured cells were taken for the photoinjection experiments by centrifuging 1 ml of the cell suspension at 1000 rpm for 1 min, and the cell pellet was re-suspended in 1 ml of the same culture medium and used as an untreated sample. The osmotic pressure was controlled by addition of mannitol with a concentration of 0.5M in the final culture medium. The TBY-2 cell sample in this condition is indicated as “mannitol treated.”

Adjunctive enzyme treatment was used for partial degradation of the cell wall. The normal culture medium was substituted with 1 ml of an enzyme solution after the centrifugation. The enzyme solution contained 0.05M MES buffer [2-(N-morpholino)ethanesulfonic acid] (Sigma-Aldrich) at pH 5.8%, 0.5% (w/v) of cellulase Onozuka RS (Serva Electrophoresis), 0.05% (w/v) of pectolyase Y-23 (Serva Electrophoresis), and 0.3M mannitol (Sigma-Aldrich). The cell suspension in the enzyme solution was kept in a dark room at 27 °C for 10 min, rinsed five times with 1 ml of 0.4M mannitol solution, and then re-suspended in 1 ml of the same culture medium containing 0.5M mannitol. This sample condition is mentioned as “enzyme treated.”

Finally, 100 µl of cell suspensions in each sample condition were placed in a glass-bottom dish (ϕ = 12 mm, Iwaki). All photoinjection experiments were done within 6 h after each treatment to maintain a healthy cell condition.

B. NIR fs laser photoinjection

The schematic illustration of the photoinjection setup is shown in Fig. 1. Amplified fs laser pulses from a regeneratively amplified fs Ti:sapphire laser system (Spectra-Physics, Solstice-Ref-MT5W, 800 nm, 150 fs) were directed into a laser-scanning confocal microscope (Olympus, IX71FVSF-2) and focused on a TBY-2 cell via a 100× oil-immersion objective lens (Olympus; Plan N, NA = 1.25). A single laser pulse was obtained using a mechanical shutter with a gate time of 1/125 s from 125 Hz pulse trains. The laser pulse energy was adjusted by using a half waveplate, polarizer, and neutral density filter. The laser beam was expanded to fill the back aperture of the objective lens, and the laser focal plane was set to the microscope image plane. The laser pulse energy through the objective lens was measured with a laser power meter (Ophir, Nova Display-Rohr). A sample was placed on a motorized microscope stage (Sigma Koki, E-65GR) placed on the microscope.

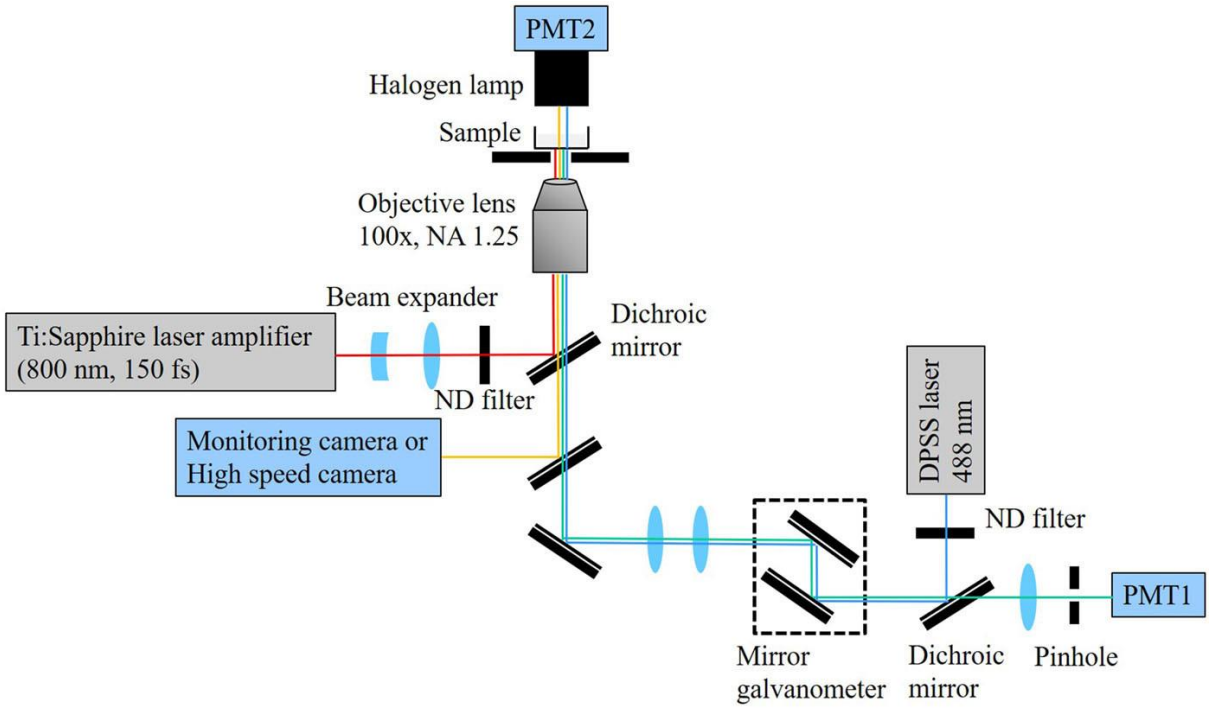

FIG. 1. *Schematic illustration of the near-infrared (NIR)-femtosecond laser system coupled with a confocal laser scanning microscope.*

C. Fluorescence measurements

Ultrabright green fluorescent nanoparticles (G-FNPs) based on copolymer of styrene and fluorescent BDPMA [boron-dipyrromethene (BODIPY) methacrylate] were used to visualize their injection into TBY-2 cells sensitively. The synthesis of G-FNPs was described elsewhere.28,29 The prepared G-FNPs (7.3 ± 0.34 × 108 particles/ml) are 80 ± 2.0 nm in diameter. This particles' volume is roughly 20 times larger than conventional DNA plasmids (2 MDa) and 400 than average proteins (30 kDa) (Fig. 2).30–32 The maximum excitation and emission wavelengths were 529 nm and 547 nm, respectively.

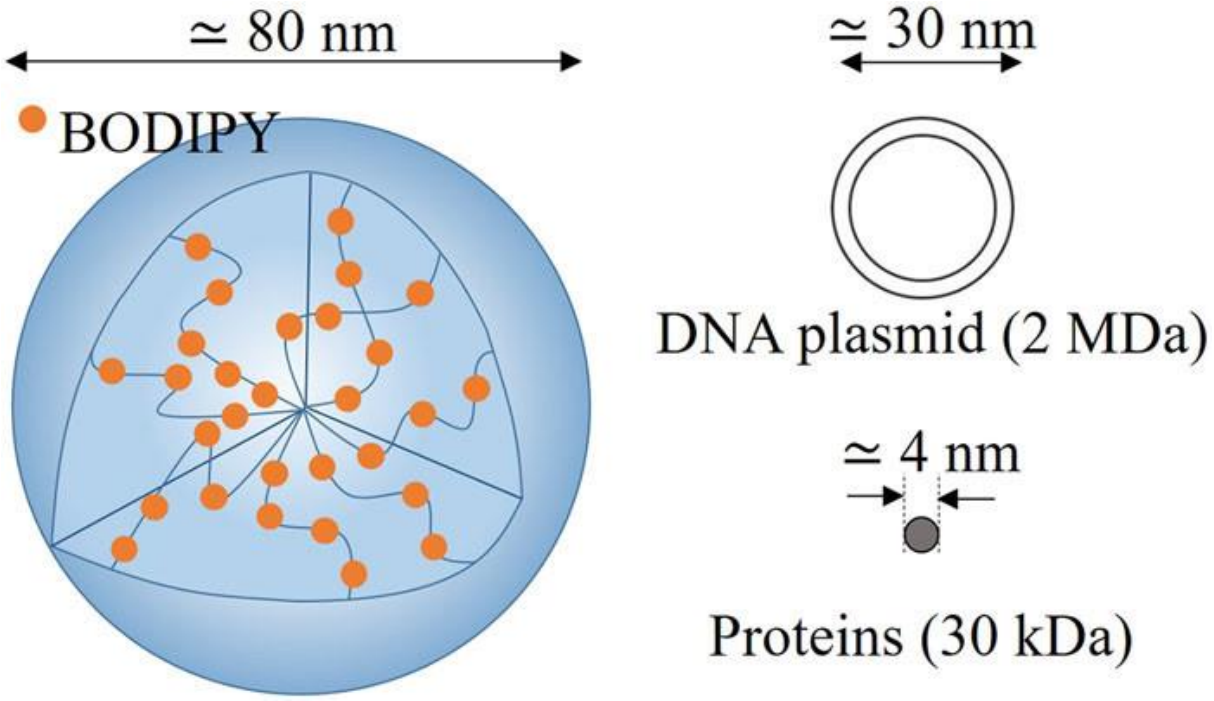

FIG. 2. *Comparison of hydrodynamic diameters among poly(styrene-co-BDPMA) nanoparticle, DNA plasmid with 2 MDa and an average protein (30 kDa).*

The G-FNP injection was observed by confocal fluorescence microscopy. A diode-pumped solid-state (DPSS) laser (Spectra-Physics, PC14763) at 488 nm wavelength was used for G-FNP excitation. 100 µl of TBY-2 cell suspension in the glass-bottom dish with 1 µl of G-FNP solution were put on the microscope stage. Same acquisition parameters were used for capturing all fluorescence images.

The G-FNP injection level was evaluated as a differential fluorescence intensity (ΔI) between before and after laser irradiation. A cytoplasmic region of a TBY-2 cell was selected using Image J software in the acquired fluorescence image. The mean intensity value before irradiation (Ibefore) was subtracted from that of 2 min after irradiation (Iafter). When laser irradiated cells were damaged, they were removed from the dataset and the ΔI histogram was made using data of 20 viable cells.

D. Cell viability assessment

Cell viability after the fs laser irradiations was assessed by the observation of cytoplasmic streaming in the transmission image and fluorescein diacetate (FDA) assay. Cytoplasmic streaming is driven from cytoskeletal myosin motion on actin filaments and transports nutrients inside the cytoplasm, thus regarding an indicator of plant cell viability. The FDA assay is a common cell viability test based on the enzymatic activity of plant cells.33 When plant cells are viable, fluorescent fluorescein (λex = 494 nm, λem = 521 nm) is yielded upon hydrolysis of non-fluorescent FDA. For the FDA assay, 2 µl of 0.36 mM FDA (Dojindo) aqueous solution was added to 100 µl of TBY-2 culture medium and its fluorescence signal was acquired after 20 min by the same confocal fluorescence imaging system as the G-FNPs measurement.

III. RESULTS

A. Effect of mannitol addition and enzyme treatment on cell structures

Morphological changes in the TBY-2 cell structure after mannitol and enzyme treatment were confirmed by transmission images before fs laser photoinjection (Fig. 3). After the mannitol addition to the culture medium, the cell vacuoles contracted in the hypertonic mannitol solution and the cell membrane was separated from the cell wall, namely, a plasmolyzed state [Fig. 3(b)]. The enzyme treatment was applied adjunctively with the mannitol addition to increase the cell wall permeability for larger molecules. In a general protocol for preparing protoplast, cell walls are completely digested after about 1 h of the enzyme treatment. In contrast, no noticeable cell morphological change was observed after 10 min of the enzyme treatment [Fig. 3(c)]. Instead of being removed, the cellulose fiber network of the cell wall would be degraded partially in this moderate process. Those results are similar to our previous report.25 Then, the fs laser photoinjection was conducted under these three cell conditions: untreated, mannitol treated (plasmolyzed), and adjunctive enzyme treated conditions.

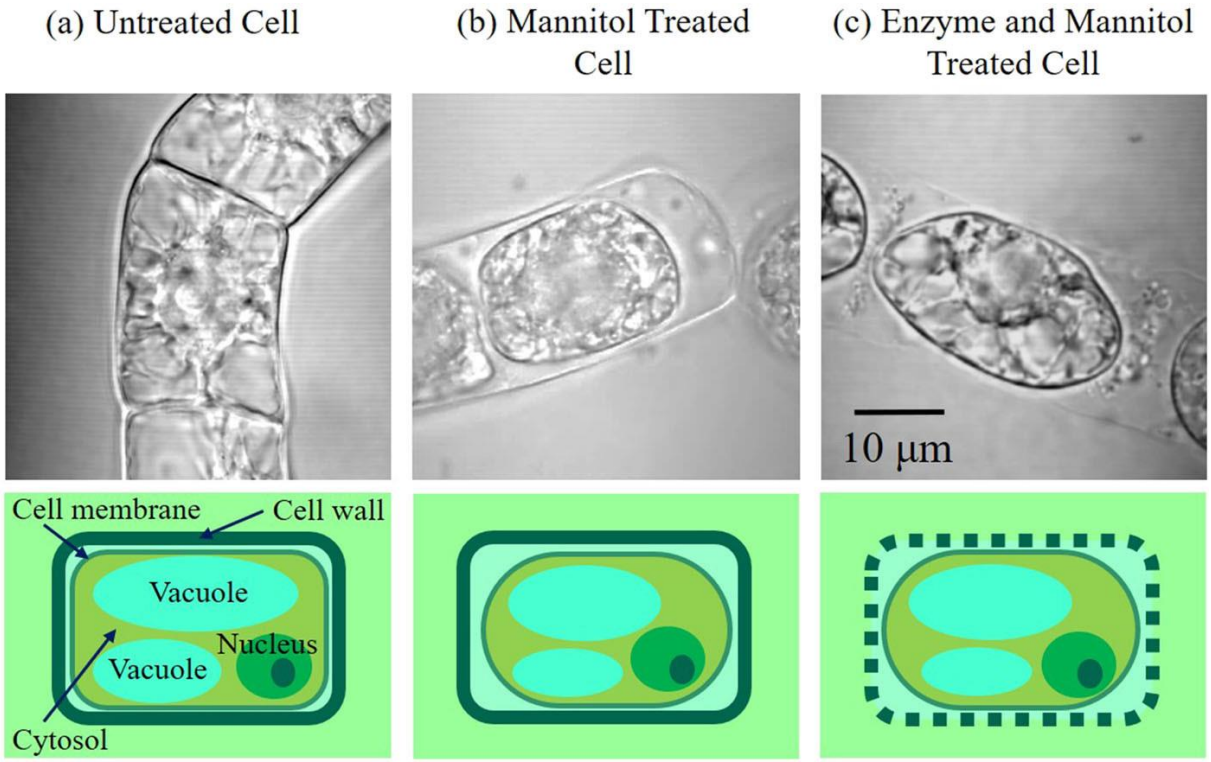

FIG. 3. *Transmission images and their schematic structures of TBY-2 cells; (a) untreated, (b) mannitol treated, and (c) enzyme and mannitol treated states. In untreated TBY-2 cells, the cell membrane is pushed against the cell wall by turgor pressure. After osmotic pressure control by mannitol addition, the turgor pressure decreased and the cell membrane is separated from the cell wall (plasmolyzed). The adjunctive enzyme treatment did not cause noticeable cell morphological change.*

B. Nanoparticles injection in the hypertonic solution and with enzyme assistance

First, the photoinjection of G-FNPs into untreated and mannitol treated TBY-2 cells was examined. Fluorescence images of the cross section of target cells were taken before and 2 min after fs laser irradiation by confocal fluorescence microscopy. A fluorescence image of untreated TBY-2 cells

before laser irradiation is shown in Fig. 4(a). There is no observable intracellular fluorescence ensuring that the nanoparticles did not diffuse into the cells spontaneously. Cell plasmolysis can be observed after the mannitol treatment from the transmission image in Fig. 4; meanwhile, the fluorescence signal could not be found within the apoplast, which is a region between the cell wall and membrane, as seen in Fig. 4(c). This observation proves that G-FNPs are too large to pass through the cell wall.

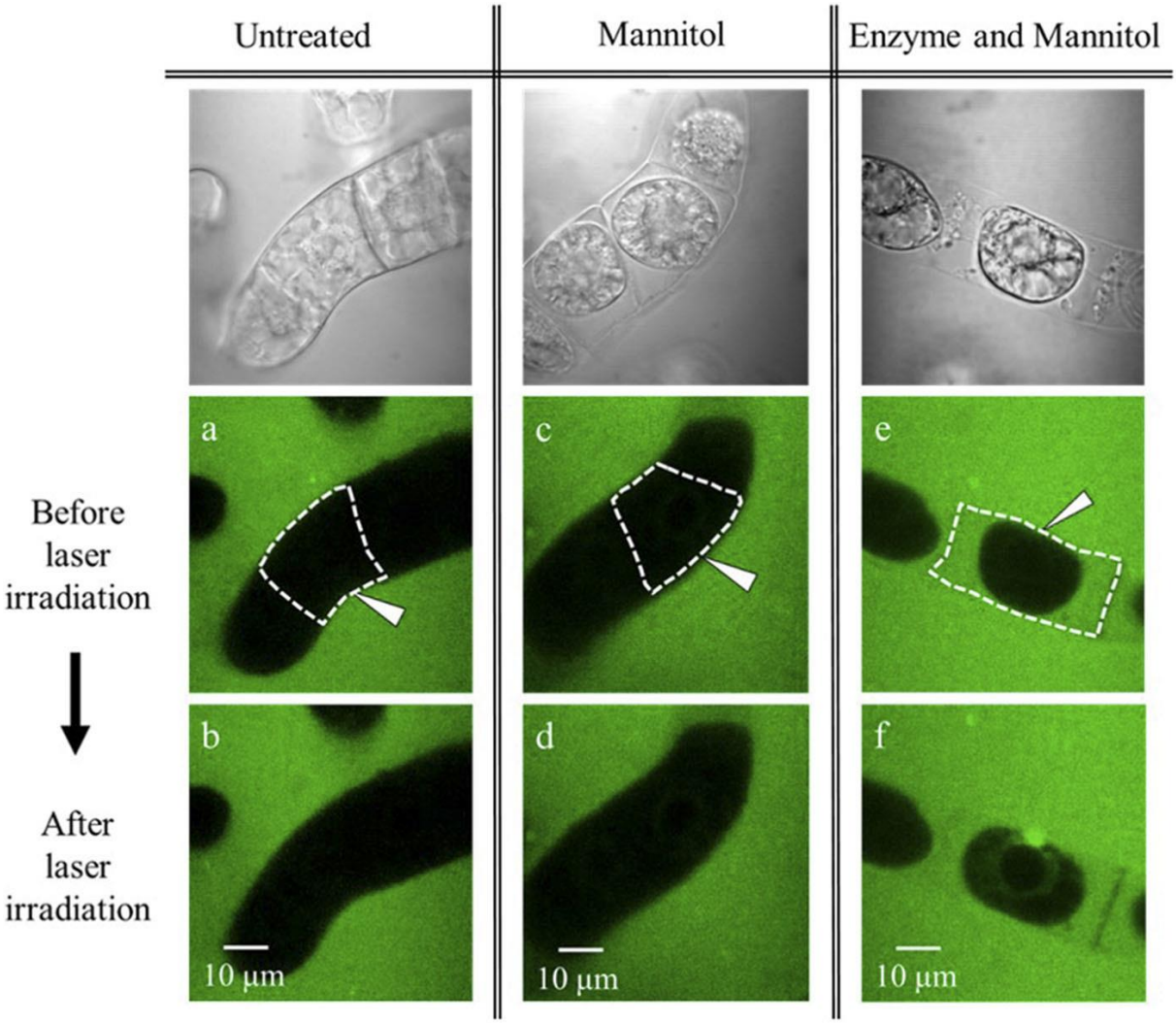

FIG. 4. *Confocal fluorescence images of [(a) and (b)] untreated, [(c) and (d)] mannitol treated and [(e) and (f)] enzyme and mannitol treated TBY-2 cells before and after fs laser irradiation under the presence of G-FNPs. The top row shows corresponding transmission images before laser irradiation. The dashed line indicates the outline of a target single cell and the white arrowheads indicate the laser focal point. These images represent the change of fluorescence intensity: (b) and (d) have no differences from (a) and (c), and (f) has a clear intensity increase compared to (e).*

A single 20 nJ fs laser pulse was then focused on the contact point of the cell wall and membrane in the medium containing the G-FNPs. The contact point was chosen as the laser focusing position for simultaneous pore formation on both the cell wall and membrane. The results for the different laser focusing positions are mentioned later. Figures 4(b)–4(d) shows representative fluorescence images of untreated and mannitol treated cells 2 min after irradiation. For untreated cells, the fluorescence

images before and after fs laser irradiation were almost identical. For mannitol treated cells, the increase in fluorescence intensity within the cytoplasm was also quite small. Thus, the G-FNP injection into the cytoplasm of untreated and mannitol treated cells was not efficient. The pore in the cell wall and membrane formed by a 20 nJ laser pulse could not be large enough for the G-FNP injection.

Next, partial degradation of the cell wall with cellulase and pectolyase was performed in order to increase the cell wall permeability for large objects with minimal damage. Figure 4(e) depicts a representative fluorescence image of adjunctive enzyme treated TBY-2 cells before irradiation in the presence of G-FNPs in the culture medium. Unlike the image shown in Fig. 4(c), fluorescence was clearly seen in the apoplast. However, the cytoplasm was always darker, indicating that the cell membrane permeability was unchanged under this condition.

In Fig. 4(f), the fluorescence image of enzyme treated TBY-2 cells 2 min after laser irradiation is presented. The fluorescence intensity increase was obviously noticed within the cytoplasm. In the meantime, auto-fluorescence increase was not detected under the same photoinjection parameter without G-FNPs in the culture medium. Therefore, it was concluded that the G-FNPs were successfully injected into the cytoplasm.

C. Injection efficiencies under three conditions

The G-FNP injection levels under untreated, mannitol treated, and adjunctive enzyme treated conditions were estimated by differential fluorescence intensities between before and after laser irradiation (ΔI). Even without laser irradiation, a small background fluorescence signal from cell's autofluorescence and/or scattered fluorescence by cells was found inside the cytoplasm. The changes in background fluorescence intensity during 2 min without laser irradiation are presented as a histogram in Fig. 5(a). The temporal fluctuations of background fluorescence for 20 cells varied from −2.25 to 1.25. The negative values were due to fluorescence bleaching throughout the laser scanning. The particle injection level is defined as ΔI, and the ΔI value of 2 is defined as injection threshold. The summary of ΔI values for 20 cells for each condition is shown as histograms in Fig. 5(b). The observations in Fig. 3 were well represented in the histograms as mentioned below.

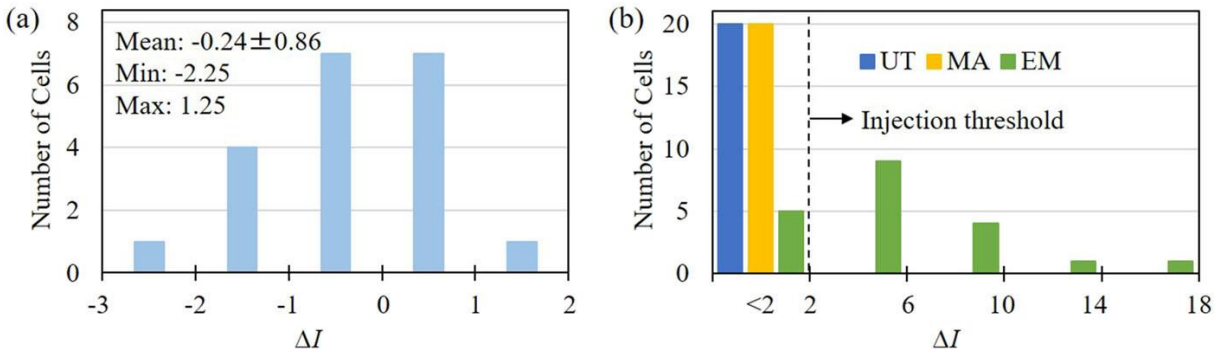

FIG. 5. *The histograms of (a) intensity changes of the background signal inside the cytoplasm in 2 min without laser irradiation, and (b) differential fluorescence intensities (ΔI) between before and after laser irradiations. Untreated (UT, blue), mannitol treated (MA, yellow) and adjunctive enzyme treated (EM, green) cells (N = 20).*

All ΔI values were less than the injection threshold for untreated and mannitol treated cells, suggesting that the G-FNPs were not able to be injected under these conditions. The adjunctive enzyme treatment shifted the ΔI distribution to a higher level than the injection threshold. Although outflow of cell contents was observed for 30% of untreated cells, as seen in transmission images (Fig. A1, supplementary material), such leakage was not observed for any mannitol and adjunctive enzyme treated cells. In addition, cytoplasmic streaming was noticed, and thus, they could be regarded as viable. Presumably, reduction of turgor pressure minimizes the cell damage by preventing cytosol leakage. The photoinjection efficiencies under the enzyme treatment with 10 nJ, 15 nJ, 20 nJ, 25 nJ, and 30 nJ pulse energies were also investigated [Figs. A2(a) and A2(b), supplementary material]. The injection efficiencies with 10 nJ and 15 nJ were very low, and they increased along with the pulse energy from 20 nJ/pulse to 30 nJ/pulse. Meanwhile, enzyme treated cells started causing cytosol leakage with 25 nJ/pulse and 30 nJ/pulse.

Long term cell viability after laser irradiation was evaluated by the FDA assay. All enzyme treated TBY-2 cells in a cell culture dish were exposed by the 20 nJ laser pulse and kept in an incubator at 27 °C for 12 h. After adding FDA in the cell culture medium, 95.7% of cells showed the fluorescence signal from fluorescein, as shown in Fig. 6(a), and the difference of the staining rate between laser irradiated cells and those without laser irradiation was very close, indicating that cells did not lose their physiological activity after the laser irradiation. Thus, photoinjection with a 20 nJ fs laser pulse under enzyme treatment was used as a standard condition hereafter.

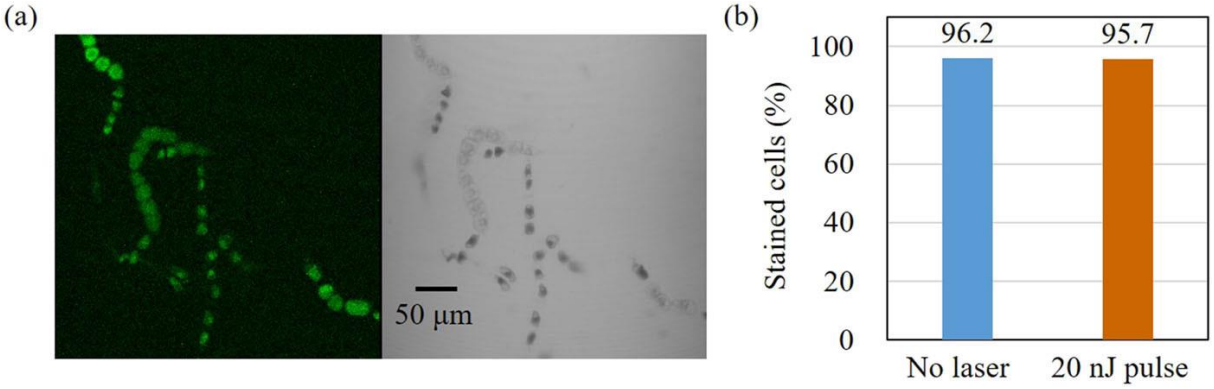

FIG. 6. *(a) Confocal fluorescence and transmission images of TBY-2 cells stained by FDA 12 h after irradiation of a single 20 nJ laser pulse. (b) The percentages of FDA-stained TBY-2 cells without laser irradiation (N = 104) and with single 20 nJ pulse laser irradiation (N = 116).*

It should be noted here that the injection of G-FNPs into the cytoplasm was also able to be observed for the plasmolyzed cells when over 30 nJ laser pulse was exerted. Therefore, the enzyme treatment is not critical for this technique. However, the injection efficiency was still quite low compared to that with enzyme treatment, and further increase in the pulse energy caused a damage for cells [Figs. A2(a) and A2(b), supplementary material]. Moreover, the additional enzyme treatment is not a big drawback because such enzyme treatment is very common in plant biotechnology.

The temporal changes in ΔI with a 20 nJ fs laser pulse under enzyme treatment were also displayed in Fig. 7. The ΔI started rising about 15 s after laser irradiation. In Fig. 4(f), G-FNPs are accumulated near the laser focal point. To understand where G-FNPs accumulate, the fs laser was focused only on the cell membrane in the presence of G-FNPs in the apoplast [Figs. A3(c) and A3(d), supplementary

material]. In this case, the accumulation also occurred around the laser focal point. Therefore, it is considered that G-FNPs are trapped not in the cell wall but in the cytoplasm, indicating that this delayed ΔI rising is due to the slower diffusion of G-FNPs in the cytoplasm than in the apoplast. The ΔI reached the maximum value in about 240 s in average, indicating that the formed pore was resealed roughly in this timescale.

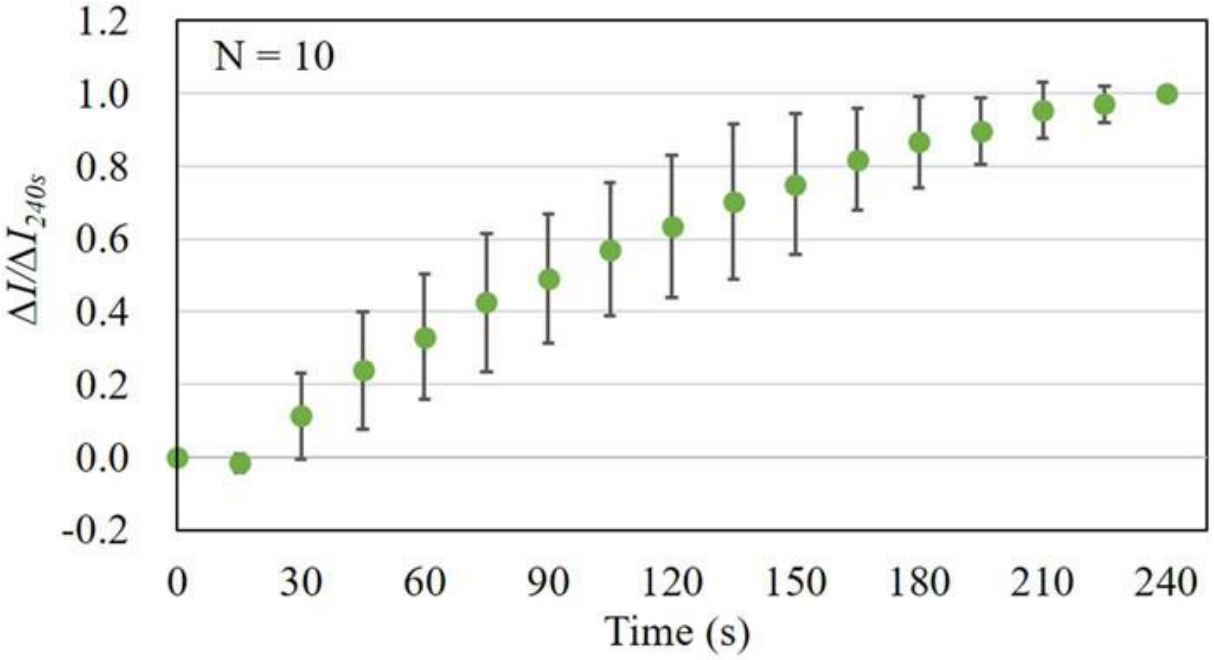

FIG. 7. *Temporal evolution of fluorescence intensity in the cytoplasm for enzyme treated cells. The graph is averaged for ten cells and normalized by the ΔI at 240 s. The error bar indicates standard deviation.*

Interestingly, even when the fs laser pulse was focused beside a cell in culture medium, injection of G-FNPs was still observed. Figure 8(a) shows fluorescence images of the TBY-2 cell before and after irradiation of the fs laser pulse at 10 µm distance from the cell wall. Fluorescence intensity increase is confirmed in the image, although the injection efficiency was lower compared to the direct fs laser irradiation, as seen in Fig. 8(b). For other laser focusing positions, we also examined at 10 µm distance from the cell membrane in the apoplast [Figs. A3(a) and A3(b), supplementary material]. In this case, G-FNPs were injected into the cytoplasm with a similar injection efficiency to the case when the laser was focused 10 µm outside the cell wall. G-FNP accumulations were observed on the nearest part of the cell membrane from the laser focal point. We even examined the laser irradiation in the cytoplasm although cells would have damages and not suitable as an injection method. G-FNPs were injected very efficiently and accumulated at a broad area on the cell membrane [Figs. A3(e) and A3(f), supplementary material].

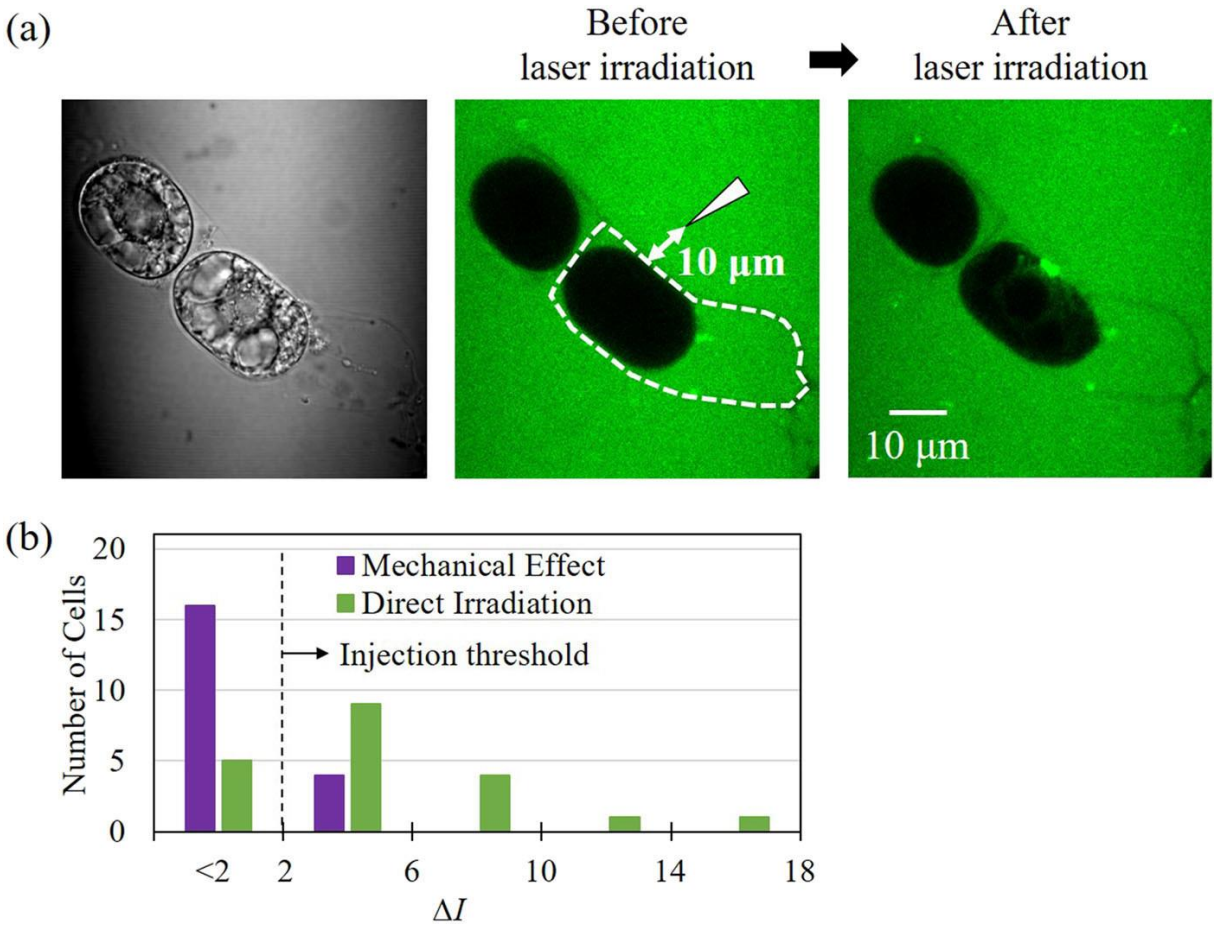

FIG. 8. *(a) Transmission and confocal fluorescence images of the enzyme treated TBY-2 cell before and after the fs laser irradiation at 10 µm distance from the cell under the presence of G-FNPs. The 20 nJ laser pulse energy was used. The dashed line indicates the outline of target single cell and the white arrowhead indicates the laser focal point. The same conditions as those in Fig. 4 were used for acquiring the fluorescence images. (b) The histogram of ΔI between before and after laser irradiations in medium beside enzyme treated cells (purple, N = 20). The case of direct irradiation is also shown as a reference (green).*

D. Transient morphological change induced by the fs laser irradiation

When the intense fs laser pulse was focused on the cell wall and membrane, laser ablation would involve the pore formation at the laser focal point and induce a tensile stress wave that propagates to the periphery.18,23 In our previous report, we suggested that such mechanical stress might be a reason why efficient injection of large molecules occurred by the photoinjection using the fs laser amplifier. Besides, we demonstrated the injection of G-FNPs by the fs laser focusing nearby TBY-2 cells without direct irradiation on the cell wall and membrane. In this case, a rapid expansion of a cavitation bubble accompanied by an impulsive hydrodynamic force spreading to the periphery can deliver mechanical force to the TBY-2 cells. Therefore, the effects of the cavitation bubble on morphological changes of TBY-2 cells were verified by high-speed imaging.

The representative transient morphological changes of TBY-2 cells by the 20 nJ fs laser pulse are shown in Fig. 9. When the fs laser pulse was focused on the cell wall [Figs. 9(a)–9(c)], the cavitation bubble generation was seen and instantaneous deformation of the cells around the laser focal point

was confirmed in their differential images as we reported elsewhere.25 Similarly, when the fs laser pulse was focused on the cell culture medium at 10 μm distance from the cell wall [Figs. 9(d)–9(f)], the cavitation bubble expanded and hit the cells, causing instantaneous deformation. This observation proved that the cells received a mechanical force from the cavitation bubble.

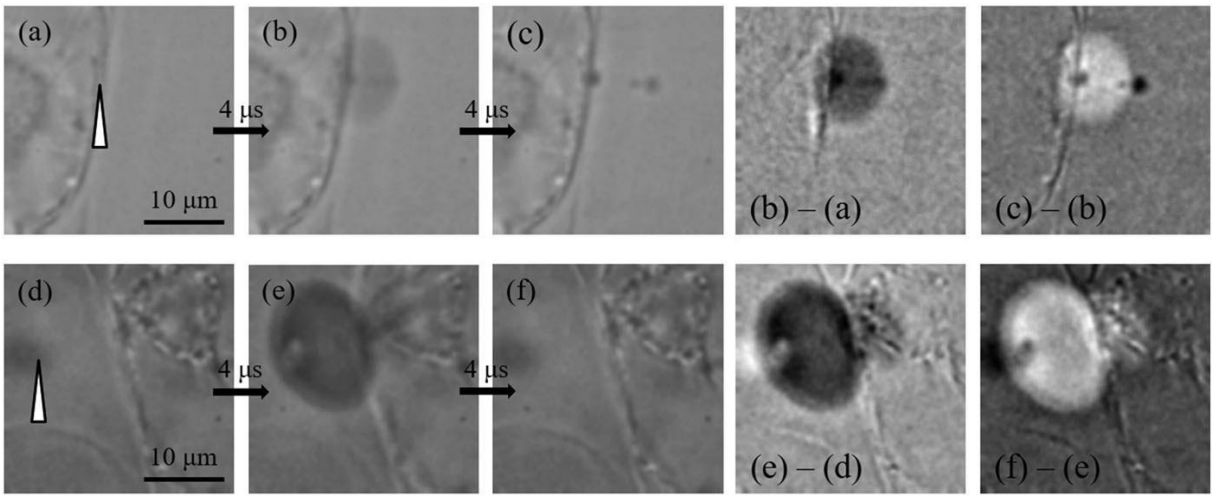

FIG. 9. *[(a)–(f)] A series of high-speed images at 4 μs intervals. White arrowheads indicate the laser focal points (a) on the contact point of the cell wall and membrane and (d) at 10 μm distance from the cell. The differential images were acquired by image calculation*

IV. DISCUSSION

The injection of G-FNPs into TBY-2 cells was achieved by employing a single intense fs laser pulse under the hypertonic condition by mannitol addition. From the transmission (Fig. 3) and fluorescence images (Fig. 4), the enzyme treatment led to the partial degradation of the network structure of the cell wall and enhanced the particle diffusion rate through the cell wall without making a protoplast. The high G-FNP concentration in the apoplast allows the efficient G-FNP injection into the cytoplasm. However, the enzyme treatment alone did not introduce G-FNPs into the cytoplasm, and the pore formation on the cell membrane by the fs laser irradiation was essential for the G-FNP injection.

Under the hypertonic condition, G-FNPs were injected when the fs laser pulse was focused on the contact point of the cell wall and membrane. With the enzyme treatment, G-FNP injection was confirmed even when the fs laser pulse was focused in the cell culture medium beside TBY-2 cells. Based on these two injection schemes, we propose mainly two mechanisms that involve the pore formation on the cell membrane.

One is a pore formation by photochemical ablation of the cell membrane. To be precise, there is no direct proof for this mechanism. However, under the laser irradiation condition, which induces breakdown of water along with the cavitation bubble as seen in Fig. 9, it is hard to consider only that the breakdown occurs without the dissociation of the cell membrane through multiphoton absorption because the absorbance of cell membrane components (e.g., proteins, lipids) at 800 nm is normally higher than that of water. Meanwhile, the pore formation using low energy and high repetition rate fs laser pulses was capable of injecting only a few nm sized molecules into plant protoplasts in the previous reports.24 Therefore, we assumed the that the photochemically induced pore was not sufficient for the injection of nanoparticles.

The second mechanism is a rupture of the cell membrane driven by photo-mechanically induced tensile stress.18 This photomechanical effect is particularly prominent with amplified intense laser pulses as higher laser energy density at the focal point results in a higher stress elevation and its rapid relaxation to the periphery.18 As seen in Fig. 9, instantaneous cell deformations were induced in both injection schemes at around the laser focal point and impact area of the cavitation bubble. In general, the plasma membrane of plant cells has less flexibility compared to that of animal cells. Therefore, a tensile stress caused by the deformation would rupture the cell membrane. This injection behavior is more clearly shown for the laser focusing on the cytoplasm. The cavitation bubble expands almost isotropically in the cytoplasm from inside cell, and the pressure would stretch the cell membrane and cause several breaks in various directions.

At last, the G-FNP injection efficiency looks lower than expected when the 40 nJ fs laser pulse forms pore on the cell wall and membrane under hypertonic condition without the enzyme treatment even though that can lead to a leakage from the cytoplasm. We consider that the softened cell wall by the enzyme treatment would have a role to intensify the mechanically induced deformation that accelerates G-FNP injection from a small pore. Without the enzyme treatment, propagation of the tensile stress at the laser focal point and deformation of the cell membrane might be restricted by the rigid cell wall.

V. CONCLUSION

The photoinjection of fluorescent nanoparticles into the cytoplasm of single plant cells with cell walls was successfully demonstrated by applying the fs laser amplifier. The injection of nanoparticles shall have a great impact since they can have specific surface properties or functional molecule delivery ability. The combination of the precise targeting capability of the fs laser photoinjection and smart nanoparticles would be a significant breakthrough that opens wide opportunity for the study of plant biology and genetic engineering. Moreover, contribution of the mechanical effect of the intense fs laser pulse on the cell membrane to the nanoparticle injection was confirmed. However, precise states of the cell membrane or cell wall after the laser irradiation or the impact of cavitation bubble (e.g., formed pore size and shape) are still under discussion. Understanding of the exact photomechanical action of amplified fs laser pulses on biological membrane would offer new perspectives in its application in biophotonics.

SUPPLEMENTARY MATERIAL

See the supplementary material for the transmission image of a damaged cell and G-FNPs injection depending on the laser pulse energies and focusing positions.

ACKNOWLEDGMENTS

This work was supported, in part, by the Grant-in-Aid for Scientific Research (C) (Grant No. JP18042069), Scientific Research on Innovative Areas (Grant No. JP18H05493) from the Japan Society for the Promotion of Science (JSPS). The collaboration between Japan and France was supported by JSPS and MEAE-MESRI under the Japan-France Integrated Action Program (PHC Sakura 40951TG).

REFERENCES

1 P. Wang, E. Lombi, F.-J. Zhao, and P. M. Kopittke, Trends Plant Sci. **21**, 699 (2016).
2 M. H. Siddiqui, M. H. Al-Whaibi, M. Firoz, and M. Y. Al-Khaishany, in Nanotechnology and Plant Sciences, edited by M. H. Siddiqui, M. H. Al-Whaibi, and F. Mohammad (Springer, Cham, 2015), Chap. II, p. 19.
3 I. Sanzari, A. Leone, and A. Ambrosone, Front. Bioeng. Biotechnol. **7**, 120 (2019).
4 D. K. Tripathi, Shweta, S. Singh, S. Singh, R. Pandey, V. P. Singh, N. C. Sharma,S. M. Prasad, N. K. Dubey, and D. K. Chauhan, Plant Physiol. Biochem. **110**, 2 (2017).
5 E. Corredor, P. S. Testillano, M.-J. Coronado, P. Gonzalez-Melendi, R. Fernandez-Pacheco, C. Marquina, M. R. Ibarra, J. M. de la Fuente, D. Rubiales, A. Perez-de-Luque, and M.-C. Risueno, BMC Plant Biol. **9**, 45 (2009).
6 F. J. Cunningham, N. S. Goh, G. S. Demirer, J. L. Matos, and M. P. Landry, Trends Biotechnol. **36**, 882 (2018).
7 S. Martin-Ortigosa, J. S. Valenstein, V. S.-Y. Lin, B. G. Trewyn, and K. Wang, Adv. Funct. Mater. **22**, 3576 (2012).
8 A. L. Rivera, M. Gomez-Lim, F. Fernandez, and A. M. Loske, Phys. Life Rev. **9**, 308 (2012).
9 D. Donmez, O. , Sim, sek, and Y. Aka Kacar, Int. J. Environ. Agri. Res. **2**, 115 (2016).
10 A. Q. Rao, A. Bakhsh, S. Kiani, K. Shahzad, A. A. Shahid, T. Husnain, and S. Riazuddin, Biotechnol. Adv. **27**, 753 (2009).
11 P. E. Vanegas, M. Valdez-Morales, M. E. Valverde, A. Cruz-Hernandez, and O. Paredes-Lopez, Plant Cell Tissue Organ Cult. **84**, 359 (2006).
12 U. K. Tirlapur and K. Konig, Nature **418**, 290 (2002).
13 D. Stevenson, B. Agate, X. Tsampoula, P. Fischer, C. T. A. Brown, W. Sibbett, A. Riches, F. Gunn-Moore, and K. Dholakia, Opt. Express **14**, 7125 (2006).
14 A. Uchugonova, K. Konig, R. Bueckle, A. Isemann, and G. Tempea, Opt. Express **16**, 9357 (2008).
15 A. A. Davis, M. J. Farrar, N. Nishimura, M. M. Jin, and C. B. Schaffer, Biophys. J. **105**, 862 (2013).
16 T. Maeno, T. Uzawa, I. Kono, K. Okano, T. Iino, K. Fukita, Y. Oshikawa, T. Ogawa, O. Iwata, T. Ito, K. Suzuki, K. Goda, and Y. Hosokawa, Sci. Rep. **8**, 8271 (2018).
17 M. Libault, L. Pingault, P. Zogli, and J. Schiefelbein, Trends Plant Sci. **22**, 949 (2017).
18 A. Vogel, J. Noack, G. Huttman, and G. Paltauf, Appl. Phys. B **81**, 1015 (2005).
19 Y. Hosokawa, S. Iguchi, R. Yasukuni, Y. Hiraki, C. Shukunami, and H. Masuhara, Appl. Surf. Sci. **255**, 9880 (2009).
20 Y. Hosokawa, H. Ochi, T. Iino, A. Hiraoka, and M. Tanaka, PLoS One **6**, e27677 (2011).
21 M. Schomaker, D. Heinemann, S. Kalies, S. Willenbrock, S. Wagner, I. Nolte, T. Ripken, H. M. Escobar, H. Meyer, and A. Heisterkamp, J. Nanobiotechnol. **13**, 10 (2015).
22 M. Li, T. Lohmuller, and J. Feldmann, Nano Lett. **15**, 770 (2015).
23 M. L. LeBlanc, T. R. Merritt, J. McMillan, J. H. Westwood, and G. A. Khodaparast, Opt. Express **21**, 14662 (2013).
24 C. A. Mitchell, S. Kalies, T. Cizmar, A. Heisterkamp, L. Torrance, A. G. Roberts, F. J. Gunn-Moore, and K. Dholakia, PLoS One **8**, e79235 (2013).
25 T. I. Rukmana, G. Moran, R. Meallet-Renault, M. Ohtani, T. Demura, R. Yasukuni, and Y. Hosokawa, Sci. Rep. **9**, 17530 (2019).
26 H. Schinkel, P. Jacobs, S. Schillberg, and M. Wehner, Biotechnol. Bioeng. **99**, 244 (2008).
27 T. Nagata, Y. Nemoto, and S. Hasezawa, Int. Rev. Cytol. **132**, 1 (1992).
28 C. Grazon, J. Rieger, R. Meallet-Renault, G. Clavier, and B. Charleux, Macromol. Rapid Commun. **32**, 699 (2011).
29 C. Grazon, J. Rieger, R. Meallet-Renault, B. Charleux, and G. Clavier, Macromolecules **46**, 5167 (2013).
30 D. D. Dunlup, A. Maggi, M. R. Soria, and L. Monaco, Nucleic Acids Res. **25**, 3095 (1997).
31 E. Dauty, J.-P. Behr, and J.-S. Remy, Gene Ther. **9**, 743 (2002).
32 N. S. Bhise, R. B. Shmueli, J. Gonzalez, and J. J. Green, Small **8**, 367 (2012).
33 K. H. Jones and J. A. Senft, J. Histochem. Cytochem. **33**, 77 (1985).